Theoretical Chemistry Accounts (2021) 140:156
https://doi.org/10.1007/s00214-021-02855-5

REGULAR ARTICLE

Effect of donor and acceptor on optoelectronic properties of benzo[1,2-b:4,5-b′]dithiophene

Kashifa Fazl-Ur-Rahman[1] · Divya Maldepalli Govindachar[1] · Ganga Periyasamy[1]

Received: 20 May 2021 / Accepted: 24 October 2021 / Published online: 6 November 2021

Abstract

A series of acceptor and donor groups anchored to benzo[1,2-b:4,5-b′]dithiophene (BDT) molecule have been systematically investigated at the density functional theory (DFT) and time-dependent density functional theory (TDDFT) level to reveal structure–property relationships, charge transfer, and fluorescence lifetimes. The DFT optimization shows that the hetero atom in the ring induces the polarity from central ring to both ends of the thiophene ring, participating in the conjugation. The donor and acceptor groups were anchored at the terminals of the BDT at two different positions to fine-tune the properties according to the requirement and study the push–pull effect. All the models studied in this work retain their aromaticity as estimated from NICS(0) and NICS(1) aromaticity index in ground and excited states. The results show that the hardness, softness, HOMO–LUMO gaps, ionization potentials (IP), and electron affinities (EA) of the BDTs are significantly affected by the electron-withdrawing and electron-donating groups. The ^{1}H and ^{13}C NMR chemical shift values have been computed to quantify the push–pull effect. Further, the charge transfer properties in these BDTs were explored based on reorganization energies and diagnostic descriptors derived from hole–electron theory that present different electron excitation behavior. The relationship between the computed variables such as highest occupied molecular orbital, lowest unoccupied molecular orbital, oscillator strength, dipole moment, absorption, and fluorescence energy correlates the system with one another and also to extend the possible applications of the system in optical devices. Structure–property relationship of various BDTs reveal that, upon optical excitation, the resonance effect plays an important role changing the bonding character between the substituent and BDT unit, enabling efficient electron delocalization. The examination of TDDFT results indicates that among the various models studied in this work, nitro-substituted model is better candidate for optoelectronic properties with relatively large absorption wavelength and long fluorescence lifetime.

Keywords TDDFT · DFT · BDT · Charge transfer · Push–pull effect · Structure–property relationship

1 Introduction

Organic molecules with a delocalized π-electron system have drawn significant advantages for their high efficiency, flexibility, and unique features where the functional groups can be substituted and the properties can be tuned easily according to the requirements [1]. Significant efforts have been focused on studying the electronic and structural properties of donor–acceptor (D–A)-substituted conjugated π-electron systems with an intention to use them in light harvesting, data processing application, modern communication, and photonic technologies [2–7]. Benzo-fused heterocycles are a class of organic chromophores where the electron-donating and electron-accepting nature of the side chain or functional group can alter the energy gap appropriately, which contribute to efficient intramolecular charge transfer (ICT) and thus improve charge transport [8]. The hetero-aromatic system end-capped with an electron acceptor (A) and an electron donor (D) widely represent a class of systems known as push–pull molecules. They have gained much attention due to their remarkable feature in material science especially in the field of nonlinear optics, optoelectronics, and their efficient charge transfer properties [9, 10]. The development of organic π-conjugated donor–acceptor–donor (D–A–D) systems composed of thiophenes (donor) and electron-deficient molecule (phenyl) provides an efficient approach to increase the absorption band through intramolecular charge transfer

✉ Ganga Periyasamy
ganga.periyasamy@gmail.com

[1] Department of Chemistry, Bangalore University, Bangalore, Karnataka 560056, India

(ICT) [11]. This approach offers a better matchup of the solar spectrum and thus attains the high efficiency in photovoltaic cells (PVC) [12]. Recently, many researchers [13, 14] have demonstrated that the incorporation of heteroatoms and the side chain into the π-conjugated electron-deficient five-membered ring causes push–pull effect that alters their electronic properties [7].

Generally, ICT occurs in push–pull systems containing electron donor and electron acceptor [15]. The ICT in these D–A systems leads to distinct optical and electronic properties. By suitable combination of the donor and acceptor groups, the ICT character of the push–pull system can be controlled [16]. The combination of donor and acceptor components affects the frontier orbital levels, thereby making them appropriate candidate materials to tune the optoelectronic properties [16]. Usually, electron donors are substituents with inductive (+I) effects such as CH_3, NH_2, OH, and benzo-fused thiophenes, whereas the electron acceptors represent substituents with inductive (−I) effects such as NO_2, CN, CHO, COOH, CF_3, etc. [9]. Resonance effect in substituents also plays an important role by participating in the π-conjugated network of the main chromophore upon photoexcitation [17]. Typical substituents include amino groups and sub-conjugated systems which form extended conjugation with the main chromophore such as CHO, $COCH_3$, COOH, C_6H_5, and thiophene.

The study reports the effect of introducing various electron donor and acceptor groups to the benzo[1,2-b:4,5-b′] dithiophene (BDT) unit on the electronic, optical, redox, and charge transfer properties at a microscopic level. Among many chromophores, BDT [10, 18] derivatives are appropriate candidate in optoelectronic devices owing to their high electron density and planar structure. In this regard, organic push–pull systems are designed with the various donors and acceptors attached to BDT molecule, and the comprehensive structure and photoelectric properties are studied using the density functional theory and time-dependent density functional theory methods [16, 19, 20]. The D–A structure is created by breaking the delocalization pattern by introducing donor and acceptor at the two thiophene rings. In the present study, a series of BDTs with different electron acceptor groups at ortho (conformer **a**)- and meta (conformer **b**)-position to the sulfur atom in the thiophene rings have been investigated. This approach can efficiently fine-tune the "push–pull" effect of BDTs, by simply changing substituents according to their varying electron-donating or electron-withdrawing power. The frontier molecular orbitals, HOMO–LUMO energy gaps, absorption and emission spectra, reorganization energies, and charge transfer have also been investigated. Further natural population analyses have been carried out to understand the nature of delocalization and ground state interactions. The ^{1}H and ^{13}C NMR chemical shift, vibrational frequency, and nucleus-independent chemical shift (NICS) calculations support the structure and push–pull character of these BDTs.

2 Computational methods

Various ortho- and meta-substituted BDT models are generated with different donor and acceptor groups. All the models were optimized in gas phase without any constraints at the tight convergence criteria using long-range corrected CAM-B3LYP [21, 22] hybrid functional and 6-31 + G(d,p) all-electron basis set for all atoms as implemented in the Gaussian 09 package [22]. The minima nature of the structure is confirmed from the computed real frequencies based on the harmonic vibrational analysis. The charge distribution in all optimized BDT models are investigated by the natural orbital method [23, 24]. The charge distribution is considered by dividing the BDT into different ring units (ring A: thiophene unit attached to donor substituent, ring B: central fused benzene unit, and ring C: thiophene unit attached to acceptor substituent), and at donor and acceptor substituents, respectively, as in Fig. 1. The oxidation and reduction properties of the BDT models were studied by calculating the vertical and adiabatic ionization potential (VIP and AIP), vertical and adiabatic electron affinity (VEA and AEA), and reorganization energy for oxidation and reduction (λ_{ele} and λ_{hole}) process using the equations given below,

$$\mathrm{VIP} = E'_{(N-1)} - E_{(N)}$$

$$\mathrm{AIP} = E_{(N-1)} - E_{(N)}$$

$$\mathrm{VEA} = E'_{(N+1)} - E_{(N)}$$

$$\mathrm{AEA} = E_{(N+1)} - E_{(N)}$$

$$\lambda_{ele} = \mathrm{AEA} - \mathrm{VEA}$$

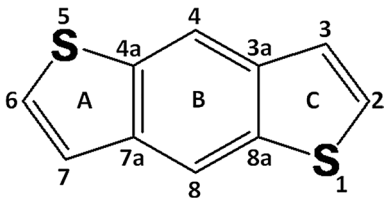

Fig. 1 Schematic representation of benzo[1,2-b:4,5-b′]dithiophene (BDT) core considered in this work. The ortho (positions 6 and 2)- and meta (positions 7 and 3)-position in the thiophene ring are substituted with various substituents [donor: CH_3, NH_2, and OH; acceptors: CF_3 (**1a/1b**), NO_2 (**2a/2b**), CN (**3a/3b**), COOH (**4a/4b**), and CHO (**5a/5b**)]. The skeletal atoms and ring labels used for NPA, NICS, ^{1}H and ^{13}C NMR calculations are shown

$$\lambda_{\text{hole}} = \text{AIP} - \text{VIP}$$

where $E_{(N)}$ is the energy of an optimized neutral molecule with N electrons, $E'_{(N\text{-}1)}$ is the energy of a cation present at optimized neutral geometry, $E_{(N\text{-}1)}$ is the energy of an optimized cation with $(N-1)$ electrons, $E'_{(N+1)}$ is the energy of an anion present at optimized neutral geometry, and $E_{(N+1)}$ is the energy of an optimized anion with $(N+1)$ electrons.

Hardness (η) and softness (σ) are related to the energy gap between highest occupied molecular orbital (HOMO) and lowest unoccupied molecular orbital (LUMO) calculated by the equations given below [25],

$$\text{Hardness, } \eta = \frac{\text{HOMO} - \text{LUMO}}{2}$$

$$\text{Softness, } \sigma = \frac{1}{\eta}$$

Nucleus-independent chemical shift (NICS) [26] values were calculated for the optimized ground and excited state geometries at CAM-B3LYP/6-31 + G(d,p) level of theory using the gauge-independent atomic orbital method (GIAO) [27] method. The NICS(0) and NICS(1) values were measured as a negative magnitude of isotropic chemical shielding values (in ppm) [26] by placing the ghost atoms at the center of the ring plane and 1 Å above this point. ^{1}H and ^{13}C NMR chemical shielding values are calculated in GIAO method by considering tetramethyl silane as reference at the same level of theory. The electron–hole distribution, electron density difference (EDD), charge transfer (CT) length, and C_{hole} and C_{ele} (centroids of hole and electron) were all generated and visualized by the Multiwfn 3.8 program [28–30].

The first vertical excitation energy corresponding to the lowest absorption energy (E_{abs}) based on the optimized ground state geometry (S_0) was calculated by the TDDFT method [31, 32]. According to Kasha's rule [33], the emission energy (E_{flu}) is determined as the $S_1 \rightarrow S_0$ transition, where the first singlet excited state (S_1) is typically important to emit fluorescence and is obtained by optimizing the S_1 state. The Stokes shift is calculated as the difference between the lowest absorption and emission energy.

3 Results and discussion

3.1 Electronic structural and optical properties of 1,5-dihydros-indacene and benzo[1,2-b:4,5-b′]dithiophene chromophore

The 1,5-dihydros-indacene and benzo[1,2-b:4,5-b′]dithiophene molecules were optimized to understand the influence of sulfur atom in the ring. The presence of sp^3 carbon in 1,5-dihydros-indacene makes the structure non-planar with bond distance of C_{sp^3}-C_{sp^2} (1.51 Å) and C_{sp^2}-C_{sp^2} (1.34–1.47 Å). Computed natural charges show intramolecular charge transfer from center of the ring to terminal rings (Fig. 2). Further, the computed NICS(0) and NICS(1) values of indacene molecule indicate that five-membered rings A and C are non-aromatic with − 0.14 and − 2.99 ppm values, while six-membered ring is aromatic with − 8.26 and − 10.01 ppm values, respectively. The substitution of $–CH_2$ group by sulfur atom in BDT makes the structure planar with C–S bond distance 1.75 Å. Further, the sulfur lone pair of electron is found to participate in the conjugation (Fig. 2); as a result, the chemical stability is found to increase in BDT molecule by 0.24 eV compared to indacene molecule. The heteroatom polarizes the molecule where the negative charge is more concentrated at the central ring (− 1.03 e) compared to the terminal rings (− 0.57 e). The MO picture shows extended delocalization; as a result, the terminal thiophene rings (− 9.30 and − 7.80 ppm) and the central phenyl ring (− 10.64 and − 11.34 ppm) become aromatic with larger negative NICS(0) and NICS(1) values. TDDFT computation shows that the absorption maximum occurs at 273.97 nm for indacene and 233.82 nm for BDT. In both the molecules, absorption occurs due to $\pi \rightarrow \pi^*$ transition. The blueshift observed for BDT is the result of larger stabilization of HOMO due to hetero atom substitution. This wavelength has been further tuned by introducing the push–pull effects by substituting donor and acceptor groups at the terminal rings (ortho- and meta-position to sulfur atom).

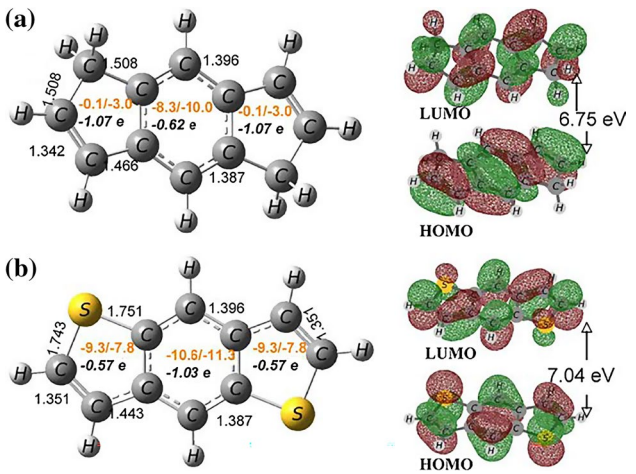

Fig. 2 Optimized molecule and molecular orbital pictures of **a** 1,5-dihydros-indacene and **b** benzo[1,2-b:4,5-b′]dithiophene (BDT). Computed bond distances (in Å), natural charges in e (***bold italics***) averaged to each rings, NICS(0) and NICS(1) (orange font in ppm) values are given

3.2 Electronic structural and optical properties of donor- and acceptor-substituted BDT

3.2.1 Structural properties

The optimized geometries of the BDT models clearly show negligible change in planarity and bond distances irrespective of the substituents size and position (Fig. 3, S1, and S2). However, the substituents enhance the intramolecular hydrogen bonding interaction between the acceptor units and the H-atoms in the ring (distances are found to vary from 2.30 to 2.77 Å, in Figs. 3, S1, and S2). These weak interactions stabilize the conformer **b** (substituent at meta-position) marginally more than conformer **a** by CH_3: 1.07–2.00 kcal mol^{-1}, NH_2: 0.46–1.05 kcal mol^{-1}, OH: 0.66–2.01 kcal mol^{-1} as mentioned in Table 1 for all substituent (NH_2-5a as an exception). Further, the intramolecular hydrogen bonding redshifted the functional group stretching frequencies of acceptor substituents in conformer **b** compared to conformer **a**. The computed vibrational frequencies of acceptor groups (υ in cm^{-1}) for all the BDT models are given in supplementary information (Table S1 in SI). The charge transfer nature, chemical reactivity, kinetic stability, chemical hardness and softness of the molecules are understood from the energy gap between the highest occupied molecular orbital (HOMO) and lowest unoccupied molecular orbital (LUMO) as given in Table 1. Among conformer **b**, the chemical stability of various donor-substituted molecules follows the trend,

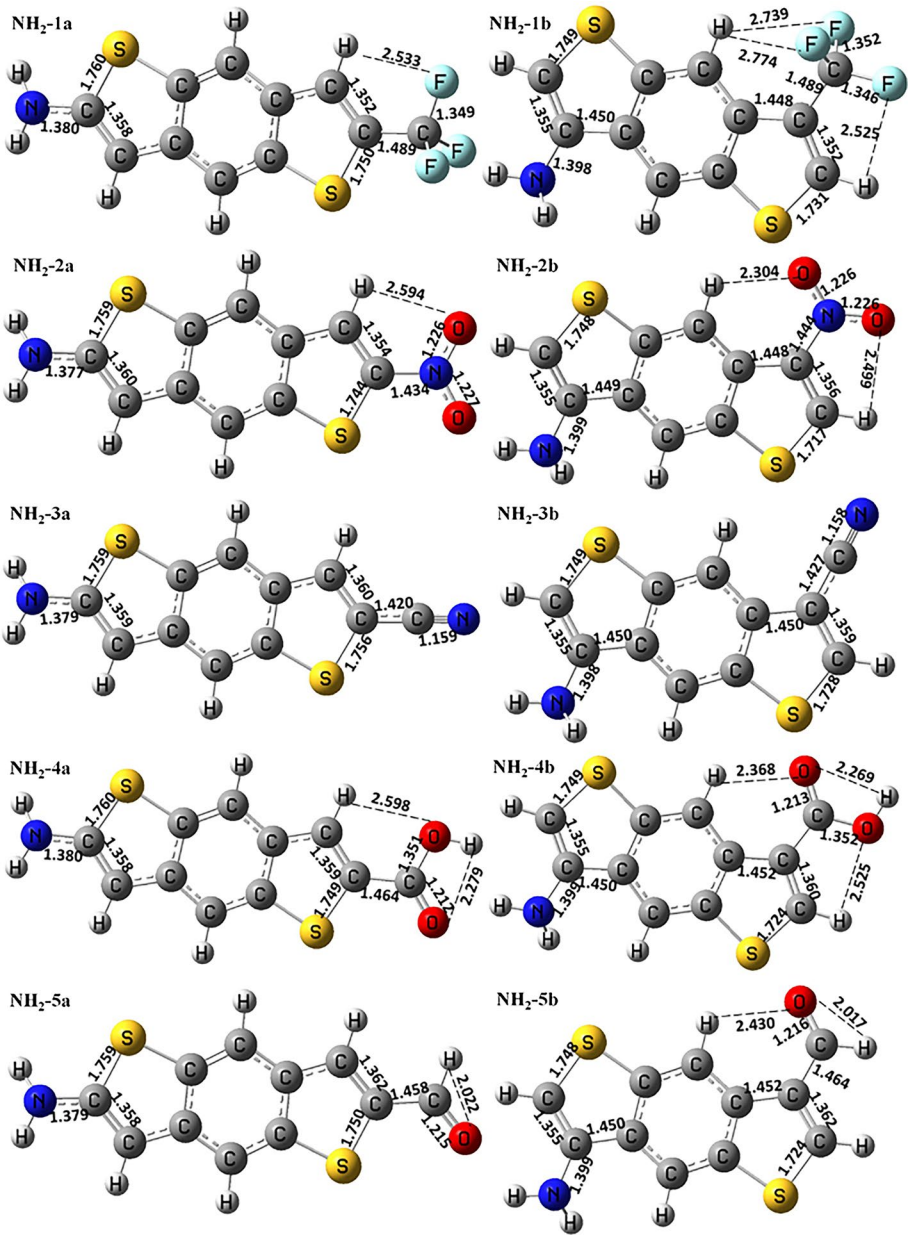

Fig. 3 Optimized geometries of various NH_2-substituted BDT models. **a** and **b** represent different conformers for the BDT models with NH_2 group anchored at positions 6 and 7, and acceptor at positions 2 and 3. The important bond distances and weak interaction (in Å) are given (**1a/1b**: CF_3, **2a/2b**: NO_2, **3a/3b**: CN, **4a/4b**: COOH, **5a/5b**: CHO). The optimized geometries of CH_3- and OH-substituted BDTs are given in supplementary information (Figs. S1 and S2)

$NH_2 < OH < CH_3$ irrespective of the acceptors. This can be explained based on the improper dihedral angle (ω) defined between donor and acceptor units as given in Table S4 in supplementary information. In CH_3-substituted BDTs, the angle ω is co-planar ~ 180° with respect to the BDT ring, and hence, there is a larger π-electron delocalization, whereas for NH_2- and OH-substituted BDTs, the angle ω deviates from co-planarity ~ 30–40° (NH_2) and ~ 30° (OH), respectively. In case of different acceptors, the NO_2-substituted models are chemically least stable and the CF_3-substituted models are chemically most stable compared to other models by 0.92 eV (NH_2), 0.89 eV (CH_3), and 0.85 eV (OH), respectively. The HOMO–LUMO gap lies over a range of 5.45–6.69 eV for conformer **b**. It is interesting to note that the absence of push–pull groups on either ends results in BDT to be chemically more stable with wide HOMO–LUMO gap (7.04 eV). The eigenfunction plots given in Fig. 4 and supplementary information Fig. S3 clearly indicate that the substitution of CH_3 as donor has negligible contribution toward HOMO and LUMO, while electron-accepting group at thiophene ring has a significant contribution. For NH_2- and OH-substituted models, the donor groups (NH_2 and OH) also show a considerable molecular orbital contribution. Specifically, CF_3 substituent has minimal contribution in HOMO and LUMO, while NO_2 group extends maximum contribution as shown in Fig. 4. As a result, CF_3-substituted BDTs has large HOMO–LUMO gap than other models studied here. Interestingly, the position of substituent is found to alter the energy gap, where ortho-substituted conformer **a** extends strong overlap than meta-substituted conformer **b**. The same phenomenon is also reflected in the hardness and softness values. The molecule **CH_3-1b** has the highest hardness value ($\eta = 3.35$ eV), and the molecules **NH_2-2a** and **NH_2-2b** are the softest molecules with $\sigma = 0.37$ eV. The computed natural charges illustrate the push–pull effect of various substituents where the polarity is stimulated at the donor and acceptor

Table.1 Computed relative energies (ΔE in kcal mol^{-1}), HOMO–LUMO energy gap (Δ in eV), natural charges (in e), hardness (η), and softness (σ) index (in eV) of various BDT models

Conformer	ΔE	Δ	Natural charges						η	σ
			Donor	Ring A	Ring B	Ring C	Acceptor	BDT		
CH_3-1a	1.620	6.648	0.060	−0.070	−0.483	−0.117	0.011	−0.071	3.32	0.30
CH_3-1b	0.00	6.694	0.052	−0.069	−0.456	−0.121	0.016	−0.068	3.35	0.30
CH_3-2a	1.831	5.615	0.063	−0.051	−0.470	0.142	−0.279	0.216	2.81	0.36
CH_3-2b	0.00	5.802	0.053	−0.056	−0.449	0.134	−0.278	0.225	2.90	0.34
CH_3-3a	1.377	6.310	0.061	−0.053	−0.481	−0.090	−0.024	−0.038	3.16	0.32
CH_3-3b	0.00	6.520	0.053	−0.060	−0.443	−0.099	−0.019	−0.034	3.26	0.31
CH_3-4a	1.066	6.168	0.059	−0.071	−0.488	−0.095	−0.010	−0.049	3.08	0.32
CH_3-4b	0.00	6.415	0.050	−0.075	−0.463	−0.082	−0.009	−0.041	3.21	0.31
CH_3-5a	1.945	5.985	0.060	−0.067	−0.494	−0.113	0.002	−0.062	2.99	0.33
CH_3-5b	0.00	6.299	0.053	−0.077	−0.472	−0.088	0.008	−0.061	3.15	0.32
NH_2-1a	1.045	6.559	−0.024	0.049	−0.487	−0.130	0.007	0.017	3.28	0.31
NH_2-1b	0.00	6.371	−0.052	0.036	−0.467	−0.121	0.016	0.036	3.19	0.31
NH_2-2a	0.815	5.423	−0.015	0.073	−0.474	0.141	−0.289	0.305	2.71	0.37
NH_2-2b	0.00	5.454	−0.052	0.057	−0.461	0.143	−0.277	0.330	2.73	0.37
NH_2-3a	0.612	6.172	−0.020	0.071	−0.486	−0.097	−0.028	0.048	3.09	0.32
NH_2-3b	0.00	6.198	−0.052	0.046	−0.456	−0.099	−0.019	0.071	3.10	0.32
NH_2-4a	0.491	6.040	−0.024	0.047	−0.495	−0.102	−0.019	0.042	3.02	0.33
NH_2-4b	0.00	6.097	−0.055	0.029	−0.453	−0.100	−0.008	0.063	3.05	0.33
NH_2-5a	0.00	5.850	−0.022	0.058	−0.490	−0.115	−0.006	0.027	2.93	0.34
NH_2-5b	0.475	6.001	−0.055	0.034	−0.451	−0.118	0.000	0.055	3.00	0.34
OH-1a	2.009	6.705	−0.182	0.187	−0.477	−0.111	0.011	0.171	3.35	0.30
OH-1b	0.00	6.518	−0.205	0.194	−0.502	−0.105	0.018	0.186	3.26	0.31
OH-2a	1.913	5.602	−0.175	0.204	−0.462	0.149	−0.282	0.457	2.80	0.36
OH-2b	0.00	5.668	−0.206	0.208	−0.495	0.148	−0.275	0.480	2.83	0.36
OH-3a	1.590	6.327	−0.179	0.202	−0.474	−0.082	−0.024	0.230	3.16	0.32
OH-3b	0.00	6.362	−0.205	0.201	−0.491	−0.084	−0.017	0.222	3.18	0.32
OH-4a	1.584	6.188	−0.182	0.183	−0.482	−0.083	−0.014	0.195	3.09	0.32
OH-4b	0.00	6.262	−0.206	−0.185	−0.487	−0.085	−0.006	0.212	3.13	0.32
OH-5a	0.660	6.002	−0.180	0.189	−0.478	−0.104	0.000	0.180	3.00	0.34
OH-5b	0.00	6.177	−0.206	0.192	−0.487	−0.099	0.002	0.204	3.09	0.32

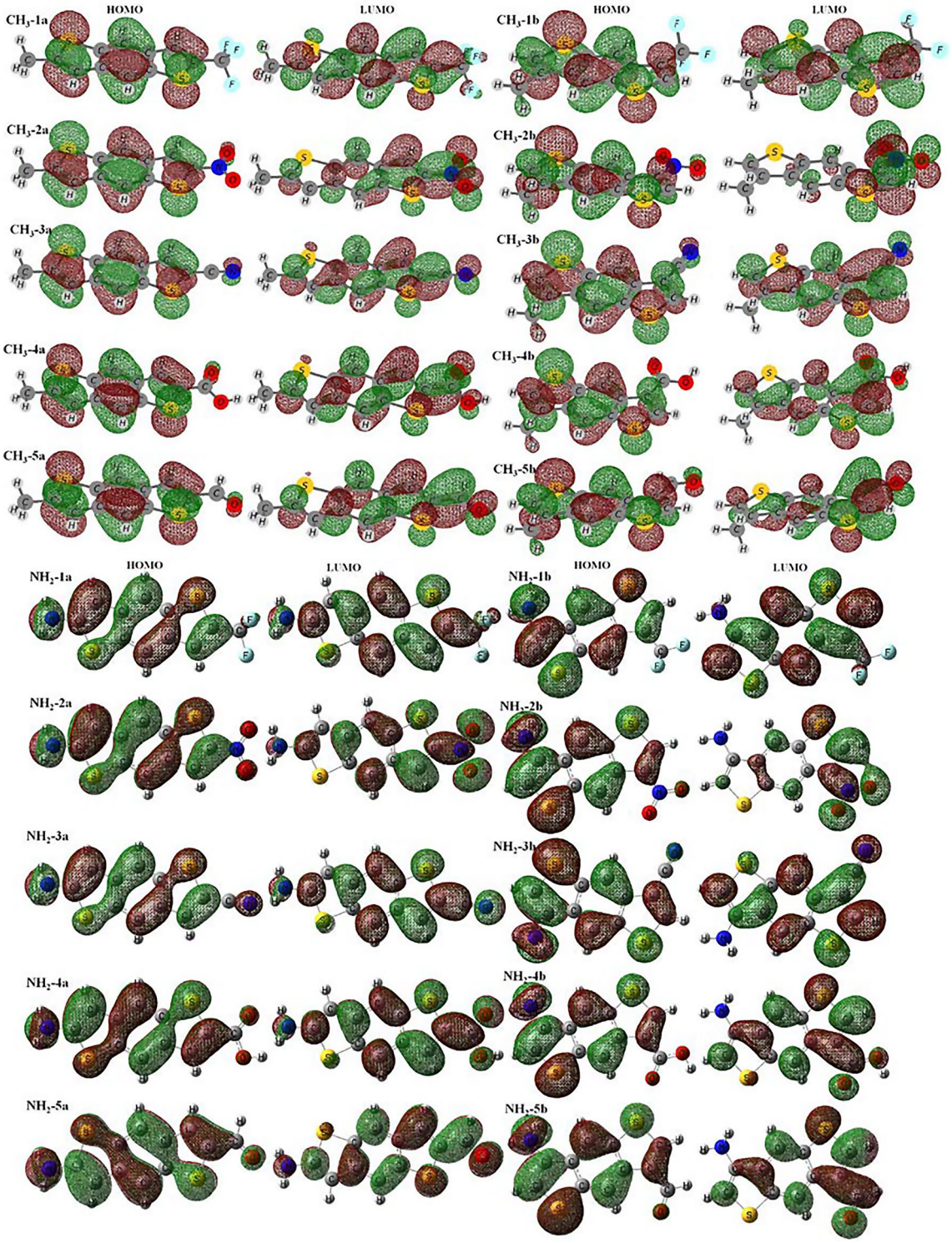

Fig. 4 Computed molecular orbital pictures of conformers **a** and **b** of various CH_3- and NH_2-substituted BDT models plotted with an isocontour value of 0.02 $Å^{-3}$. The orbital pictures of OH-substituted BDT models are given in supplementary information (Fig. S3)

ends. For CH_3-substituted BDTs, the CH_3 group exhibits a partial positive charge of 0.06 and 0.05 e at conformers **a** and **b**. The rings A and C possesses a negative charge and acts as donor units where ring C is a strong donor compared to ring A. Irrespective of the donor and acceptor substituents, the central ring B possesses an overall partial negative charge of 0.5 e and serves as a linker between rings A and C, thus stabilizing the push–pull effect at the thiophene units.

In case of NH_2- and OH-substituted BDTs, both NH_2 and OH groups possess a partial negative charge (NH_2: 0.02 e and 0.05 e at conformers **a** and **b**, OH: 0.18 e and 0.21 e at conformers **a** and **b**). Consequently, ring A display a partial positive charge while ring C exhibits a partial negative charge. This facilitates intramolecular charge transfer from one unit to another. In case of different acceptor substituents, the CF_3 and NO_2 substituents tend to cause maximum charge polarization but show an opposite behavior. The CF_3 group leads to maximum negative charge at ring C with a positive charge at CF_3 group while in contrast NO_2 results in a positive charge at ring C and a maximum negative charge at NO_2 end. When CH_3 acts as a donor, the conformer **a** is found to possess more charge at the donor end, while for NH_2 and OH, conformer **b** possesses more charge at the donor end. This indicates substituent positional effects on the nature of charge distribution for different donor moieties. Hence, the arrangement of the electron donors and acceptors around the BDT is important when designing a push–pull molecule.

Accordingly, the change in electron density distribution is reflected in the NICS values and the results are given in supplementary information (Table S2 in SI). The larger negative NICS(1) value compared to NICS(0) indicates the larger contribution from π-orbitals. Considering the aromatic character of free thiophene (− 13.6 ppm) [34], the aromatic character of rings A and C in BDT is slightly reduced as donor and acceptor substituents are anchored to thiophene units. The aromaticity of ring C is enhanced compared to that of free benzene (− 9.7 ppm) due to the push–pull effect that tend to increase the aromatic character of central fused benzene [26]. This is accounted based on the high negative charge at the ring B that increases its aromatic nature by 1–2 ppm. The NICS(0) and NICS(1) values were computed for excited geometry and a similar trend in aromaticity in the rings were observed. However, the aromatic nature is found to increase by 0.2–1 ppm during excitation. This indicates the higher delocalization at the excited state compared to the ground state. (Values for excited molecules are given in Table S2 in SI.)

Finally, the NMR chemical shielding values are calculated to check the reliability of the optimized structures, aromatic nature and to quantify the push–pull nature of these BDTs. It is important to recall that the chemical shift of protons usually shifted to high δ values due to the substitution of electron-withdrawing groups and shifted to low δ values in case of electron-donating group (Table S3 in SI). The protons in positions 4 and 8 are deshielded compared to other protons attributed to the highly aromatic six-membered ring. Further, the delocalization along with push–pull effect in the molecules is evident from the chemical shift of protons. There is a slight downfield shift of protons at positions 2 and 3 (2-H and 3-H) compared to that of protons at positions 6 and 7 (6-H and 7-H). This is due to the electron-withdrawing and electron-donating groups at rings C and A, respectively. The presence of nitro and aldehyde groups in CH_3-2b (9.79) and CH_3-5b (9.62) makes the protons (2-H and 3-H) highly deshielded with a larger chemical shift value than other BDTs. The protons of CH_3 donor are slightly deshielded in conformer **b** (3.3) compared to conformer **a** (3.2). Overall, the computed NMR chemical shift values accounts for the shielding and deshielding nature of protons due to the push–pull electronic environment in these BDTs. The ^{13}C NMR chemical shift values are given in Table S5 of supplementary information which is found to follow the same trend as ^{1}H NMR. These data are useful to validate the results by comparing with experimental data. Similar observation holds good for NH_2- and OH-substituted BDTs.

3.2.2 Ionization potential, electron affinity, and reorganization energy

Vertical ionization potential (VIP) indicates the energy required by a molecule to lose an electron and form a cation. The smaller the VIP of molecule, the more easily it loses electron and turn into a hole carrier. Vertical electron affinity (VEA) is the energy required by a molecule to accept an electron. Larger the VEA value, the more readily it accepts electron and serves as an electron transport material. The VIP and VEA of the BDT models are tabulated in Table 2. The COOH-containing BDTs show low IP compared to other molecules. The trend in VIP values observed for various donors is as follows, NH_2-4b (7.32 eV) < CH_3-4b (7.62 eV) < OH-4b (7.64 eV). The hole transport barrier varies from 0.30 to 0.38 eV (4b < 5b < 1b < 3b < 2b). The NO_2-substituted BDTs show larger VEA value in comparison with other molecules and observe to follow the order, NH_2-2a (1.24 eV) < OH-2a (1.35 eV) < CH_3-2a (1.37 eV). The electron transfer capability of the BDTs is enhanced more for conformer **a** in the presence of NO_2 group. The COOH-substituted BDTs are good hole transport materials irrespective of conformers. (IP value varies within 0.02–0.06 eV for both conformers.) The low VIP and high VEA of NO_2-substituted BDTs can be correlated based on the strong electron acceptor ability of NO_2 and hence have good charge transfer capability.

Marcus theory [35] is used effectively to predict the charge transport property of a material. According to Marcus theory, the charge transfer rate constant κ is given by,

$$\kappa = A \exp\left[\frac{-\lambda}{4K_B T}\right]$$

where A is electron coupling, T is temperature, K_B is Boltzmann constant, and λ is reorganization energy. From the above equation, an important parameter to determine charge transport is λ. The smaller the value of λ, the better

Table.2 Computed adiabatic ionization potential (AIP), adiabatic electron affinity (AEA), vertical ionization potential (VIP), vertical electron affinity (VEA), and reorganization energy for hole (λ_{hole}) and electron (λ_{ele}) in eV for various BDT conformer

Conformer	AIP	AEA	VIP	VEA	λ_{hole}	λ_{ele}
CH_3-1a	7.687	0.467	7.816	0.195	0.129	0.272
CH_3-1b	7.685	0.360	7.793	0.097	0.108	0.263
CH_3-2a	7.886	1.667	8.001	1.373	0.115	0.294
CH_3-2b	7.834	1.397	7.941	1.094	0.107	0.303
CH_3-3a	7.767	0.805	7.885	0.618	0.118	0.187
CH_3-3b	7.774	0.542	7.868	0.374	0.094	0.168
CH_3-4a	7.540	0.814	7.666	0.547	0.126	0.267
CH_3-4b	7.503	0.435	7.618	0.244	0.115	0.191
CH_3-5a	7.635	1.016	7.751	0.789	0.116	0.227
CH_3-5b	7.666	0.678	7.775	0.488	0.109	0.190
NH_2-1a	7.128	0.323	7.461	0.030	0.336	0.294
NH_2-1b	7.099	0.291	7.477	0.093	0.378	0.198
NH_2-2a	7.318	1.554	7.620	1.236	0.303	0.318
NH_2-2b	7.216	1.403	7.605	1.094	0.389	0.310
NH_2-3a	7.204	0.659	7.510	0.420	0.306	0.239
NH_2-3b	7.816	0.560	7.556	0.374	0.370	0.186
NH_2-4a	7.020	0.696	7.343	0.388	0.323	0.308
NH_2-4b	6.942	0.507	7.315	0.245	0.374	0.262
NH_2-5a	7.095	0.886	7.410	0.623	0.315	0.263
NH_2-5b	7.003	0.619	7.380	0.375	0.376	0.245
OH-1a	7.566	0.463	7.811	0.116	0.246	0.347
OH-1b	7.573	0.463	7.814	0.253	0.241	0.210
OH-2a	7.764	1.674	7.976	1.353	0.212	0.322
OH-2b	7.703	1.525	7.959	1.212	0.257	0.313
OH-3a	7.641	0.800	7.860	0.561	0.219	0.240
OH-3b	7.663	0.711	7.896	0.522	0.233	0.189
OH-4a	7.441	0.809	7.673	0.516	0.232	0.293
OH-4b	7.400	0.642	7.640	0.381	0.240	0.262
OH-5a	7.522	1.017	7.745	0.751	0.223	0.266
OH-5b	7.471	0.755	7.712	0.507	0.241	0.248

the charge transport capability. The reorganization energies are calculated for hole (λ_{hole}) and electron (λ_{ele}) using Eqs. (5) and (6), respectively, which estimate the charge transport for holes and electrons [36, 37]. The reorganization energies of hole and electron for various BDTs are listed in Table 2. The electronic reorganization energies of CN-substituted BDTs are smaller than that of other molecules and hence serve as good electron transport systems. For CH_3 donor, the hole reorganization energies of CN-substituted BDT is small compared to other molecules, whereas for NH_2 and OH donors, the NO_2-substituted BDTs of conformer **a** show small value of λ_{hole}. The electron and hole reorganization energies are comparatively small for BDTs containing CH_3 donor. The CN-containing BDTs with CH_3 donor serve as an efficient ambipolar transport system. In case of CH_3-containing BDTs, the λ_{hole} and λ_{ele} values of conformer **b** are relatively small compared to conformer **a** (except CH_3-2b).

3.2.3 Electron excitation analysis

The hole and electron distribution can be quantitatively characterized that are useful for identifying type of electron excitations. In this regard, a multitude of hole–electron descriptors were used such as $\Delta\rho$, S_r, D, q_{CT}, μ_{CT}, H, t, Δr, and Λ indices to understand the charge transfer [38–42]. Hole–electron descriptor details are given in supplementary information.

To account for the push–pull behavior and donor–acceptor nature within the BDTs during the electron excitation, multifarious descriptors based on hole–electron theory have been used (details are given in SI). The computed values in

Table 3 provide a quantitative picture on electron transition characteristics. Figures 5, S4, S5, and S6 illustrate the total density difference for ground and excited states ($\Delta\rho$), D_{CT} values, and C_{hole}/C_{ele} map. The D_{CT} value of NO_2-substituted BDT is very small (CH_3-2a: 0.996, CH_3-2b: 0.813, NH_2-2b: 0.843, OH-2a: 1.017, OH-2b: 0.818) compared to other BDTs, and the corresponding S_r index is close to 0.50 to 0.51 Å, implying that about half of hole and electron part matched perfectly. This suggests that the excitation is a typical local excitation (LE). Further, the *t* index is negative suggesting that the separation of hole and electron distributions is insignificant, which also support LE. The main electronic transition is $n \rightarrow \pi^*$ due to the lone pair of electrons and π^* orbitals on NO_2 group. Similar observations hold good for CH_3-5b and OH-5b where the D_{CT} values are slightly large 1.231 and 1.397, respectively. The corresponding S_r index is 0.50 and 0.49, and the excitation is a $\pi \rightarrow \pi^*$ (occurs on thiophene unit attached to CHO group) and $n \rightarrow \pi^*$ (on CHO group) LE. The *H* index of the above-discussed BDTs is not large as the hole and electron of these states are distributed in a local region. An exceptionally high D_{CT} value (3.915 Å) is observed for NH_2-2a with S_r index of 0.695 and a positive *t* index (1.619 Å), which obviously points to a charge transfer (CT) excitation. There is $\pi \rightarrow \pi^*$-type transition from amino group (donor) toward nitro group (acceptor), thus highlighting push–pull effect. In case of other BDTs, the distribution of hole and electron in these molecules is wider (D_{CT} value in the range 1.279 to 4.359 Å), and their S_r and *H* indices are markedly larger (S_r value varies between 0.695 and 0.841 and *H* index from 2.658 to 3.170). The electronic transitions are CT type where the direction of electron transfer is from donor end to acceptor end. However, the barycenters are not exactly on the donor or acceptor moieties, but centered on the either thiophene units, which suggests that the charge transfer occurs from thiophene unit attached to a donor to thiophene unit attached to an acceptor via fused benzene

Table.3 Hole–electron descriptors (S_r, *H*, and *t*), charge transfer length, charge and dipole moment (D_{CT}, q_{CT}, μ_{CT}), and diagnostic descriptors (Δr and Λ) of various BDTs

Conformer	Critical state	S_r (au)	D_{CT} (Å)	q_{CT} (le$^-$l)	μ_{CT} (Debye)	*H* (Å)	*t* (Å)	Δr (Å)	Λ (Å)	$d_{D\text{-}A}$ (Å)
CH_3-1a	S_1	0.824	1.279	0.46	2.843	3.145	−1.458	0.83	0.74	9.977
CH_3-1b	S_1	0.811	1.746	0.46	3.870	3.082	−0.508	1.05	0.73	7.882
CH_3-2a	S_2	0.499	0.996	0.74	3.557	1.787	−0.291	2.41	0.41	9.895
CH_3-2b	S_2	0.505	0.813	0.74	2.897	1.621	−0.292	1.71	0.43	7.883
CH_3-3a	S_1	0.805	2.306	0.49	5.444	3.170	−0.469	1.54	0.74	9.913
CH_3-3b	S_1	0.805	2.386	0.46	5.240	3.047	−0.064	1.66	0.72	7.822
CH_3-4a	S_1	0.778	2.461	0.52	6.193	3.140	−0.225	1.82	0.71	9.956
CH_3-4b	S_1	0.776	3.123	0.50	7.533	2.902	0.898	2.31	0.66	7.884
CH_3-5a	S_1	0.740	2.805	0.57	7.676	3.088	0.130	2.22	0.68	9.952
CH_3-5b	S_1	0.500	1.231	0.75	4.455	1.641	0.152	2.65	0.38	7.906
NH_2-1a	S_1	0.831	2.476	0.45	5.338	2.886	0.070	1.65	0.72	9.855
NH_2-1b	S_1	0.745	2.772	0.55	7.257	2.803	0.755	2.07	0.66	7.765
NH_2-2a	S_2	0.695	3.915	0.61	11.399	2.658	1.619	3.38	0.54	9.769
NH_2-2b	S_2	0.492	0.843	0.75	3.015	1.631	−0.267	1.70	0.43	7.766
NH_2-3a	S_1	0.806	3.640	0.47	8.224	2.854	1.214	2.30	0.70	9.791
NH_2-3b	S_1	0.730	3.328	0.55	8.775	2.757	1.282	2.65	0.64	7.704
NH_2-4a	S_1	0.779	3.601	0.51	8.776	2.898	1.114	2.59	0.68	9.834
NH_2-4b	S_1	0.726	4.003	0.54	10.232	2.756	1.981	3.16	0.58	7.767
NH_2-5a	S_1	0.759	3.780	0.54	9.769	2.858	1.345	2.90	0.65	9.828
NH_2-5b	S_1	0.705	4.359	0.55	11.528	2.665	2.432	3.50	0.53	7.790
OH-1a	S_1	0.841	1.663	0.44	3.544	2.959	−0.815	1.20	0.74	9.808
OH-1b	S_1	0.777	2.352	0.51	5.736	2.880	0.246	1.64	0.70	7.773
OH-2a	S_2	0.503	1.017	0.75	3.631	1.789	−0.263	2.32	0.42	9.724
OH-2b	S_2	0.496	0.818	0.75	2.924	1.638	−0.294	1.71	0.43	7.775
OH-3a	S_1	0.815	2.996	0.47	6.734	2.936	0.495	1.84	0.73	9.743
OH-3b	S_1	0.770	2.891	0.50	6.939	2.878	0.633	2.12	0.69	7.711
OH-4a	S_1	0.782	2.936	0.51	7.204	2.936	0.434	2.15	0.70	9.787
OH-4b	S_1	0.757	3.634	0.50	8.686	2.840	1.475	2.73	0.63	7.774
OH-5a	S_1	0.754	3.191	0.55	8.405	2.885	0.744	2.47	0.68	9.782
OH-5b	S_1	0.489	1.397	0.76	5.062	1.675	0.123	2.51	0.38	7.797

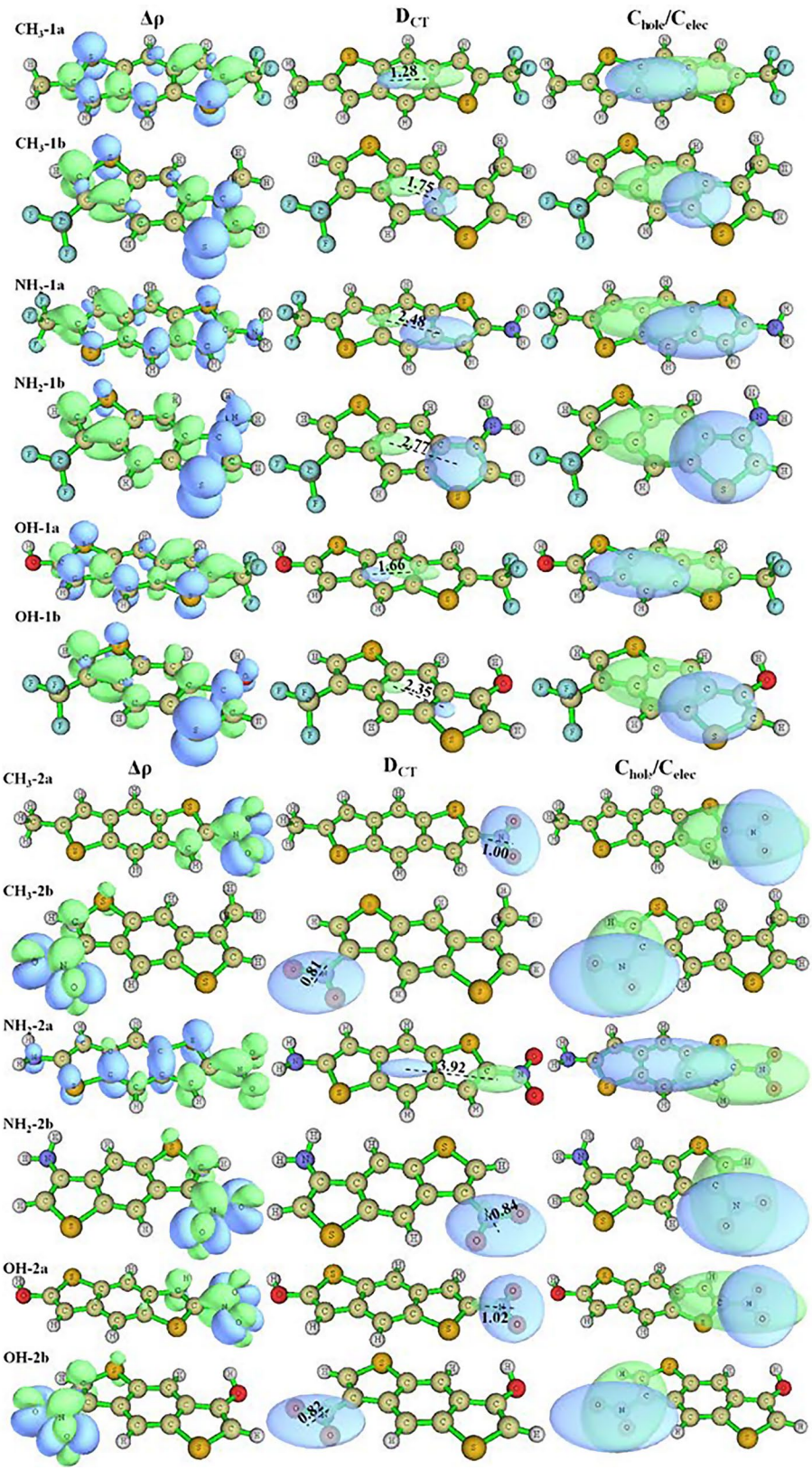

Fig. 5 Computed total density difference for ground and excited states ($\Delta\rho$, isovalue set to 0.001 Å), graphical representation of D_{CT} indicating the approximate barycenters of positive (green) and negative (blue) part obtained by increasing the isovalue accordingly and D_{CT} value is also labeled, and centroids of hole and electron (C_{hole}/C_{ele} map, isovalue set to 0.001 Å) of CF_3- and NO_2-substituted BDTs. The figures for CN-, COOH-, and CHO-substituted BDTs are given in supplementary information (Figs. S4, S5, and S6)

(Fig. 5). In the presence of NH_2 donor, all the BDTs show CT excitation (except NH_2-2b), which is accounted based on the donor–acceptor distances for NO_2-substituted BDTs where the $d_{D\text{-}A}$ values are 7.766 Å (NH_2-2b), 7.775 Å (OH-2b) and 7.883 Å (CH_3-2b), respectively. It is evident that the $d_{D\text{-}A}$ of NH_2-2b is less than that of OH-2b and CH_3-2b. The NO_2-substituted conformer **a** exhibits $d_{D\text{-}A}$ in the range OH-2a (9.724 Å) < 9.769 Å (NH_2-2a) < CH_3-2a (9.895 Å) and all of them are found to show CT excitation. Also the improper dihedral angle (ω_1) is − 40.31° for NH_2-2b which is much deviated from co-planarity compared to NH_2-2a (27.63°). Hence NH_2-2b favors LE and NH_2-2a favors CT excitation. The improper dihedral angles ω_1 and ω_2 are − 0.08 and 179.86° for CH_3-5b (exactly coplanar in case of CH_3-5a) and 30.42 and − 149.70° for OH-5b (− 15.66 and 164.40° in case of OH-5a) that suggests a deviation from planarity with respect to the BDT plane compared to conformer **a**, and hence exhibits LE. The improper dihedrals of all the optimized BDTs are listed in supplementary information (Table S4).

The Δr index ranges from 0.8 to 3.5 Å, where most of the BDTs exhibit long-range excitation ($\Delta r > 1.5$ Å) with a few exceptions such as CF_3-substituted CH_3-1a, CH_3-1b, and OH-1a ($\Delta r < 1.5$ Å). The BDTs with NH_2 donor display a strong charge transfer irrespective of the acceptors. The Λ-values of all BDTs are in the range $0.4 \le \Lambda \le 0.7$ where CH_3-2a (0.41), CH_3-2b (0.43), NH_2-2b (0.43), OH-2a (0.42), OH-2b (0.43), CH_3-5b (0.38), and OH-5b (0.38) have a relatively small overlap and other BDTs show a larger hole–electron overlapping extent.

3.2.4 Absorption spectra

TDDFT computations were carried to determine first six singlet excited states. The computed absorption spectra are given in Fig. 6. The absorption spectra clearly show that the absorption wavelength covers wide wavelength region due to push–pull groups anchored to the BDT and range roughly from 180 to 400 nm. The ability to tune the absorption at a particular wavelength is an important characteristic for optoelectronic properties. The absorption maximum has more than 65% contribution from HOMO to LUMO transition (Figs. 7, S7, S8, S9, and S10), while the transition from other delocalized frontier orbitals contribute 35% as shown in the orbital transition diagram (Figs. 7, S7, S8, S9, and S10). Overall, the excitations are mainly due to $\pi \rightarrow \pi^*$ transitions for CH_3-substituted BDTs, whereas $\pi \rightarrow \pi^*$ and $n \rightarrow \pi^*$ transitions are notable for NH_2- and OH-substituted BDTs. The push–pull effect increases the absorption wavelength for all models as expected when compared to the unsubstituted one ($\lambda_{max} = 200$ nm). Among the models explored, NO_2-substituted BDTs absorb at higher wavelength and follows the order OH-2a (352.58 eV) < CH_3-2a (356.93) < NH_2-2a (361.66) while CF_3-substituted ones absorbs at lower wavelength and the observed trend is OH-1a (287.42) < NH_2-1a (292.03) < CH_3-1a (294.02) in eV. In case of CH_3 donor, irrespective of the nature of acceptor groups, the conformer **a** is markedly redshifted compared to conformer **b**. This is due to the strong overlap between sulfur lone pair and donor/acceptor substituents in conformer **a**. The computed absorption maxima are well correlated with the calculated HOMO–LUMO energy gaps. The HOMO–LUMO gap is large and small for CF_3- and NO_2-substituted BDT molecules which is responsible for the marked blueshift and redshift in the absorption spectra of these BDTs. The oscillator strengths are highest for the cyano-substituted conformer **a** and follow the trend $NH_2 > OH > CH_3$, due to strong electron-withdrawing effect of CN unit. The least oscillator strengths are observed for nitro-substituted conformer **b** and tend to follow the order $NH_2 < OH < CH_3$ that suggests weak electron-withdrawing effect of NO_2 unit in these conformers. The trend in oscillator strengths observed for various acceptors is as follows, $CN > COOH > CHO > NO_2 > CF_3$ (**CH_3-a**), $CN > CHO > COOH > NO_2 > CF_3$ (**NH_2-a**), $CN > COOH > CHO > NO_2 > CF_3$ (**OH-a**), $CN > COOH > CHO > CF_3 > NO_2$ (**CH_3-b**), $CN > COOH > CHO > CF_3 > NO_2$ (**NH_2-b**), and $CN > CF_3 > COOH > CHO > NO_2$ (**OH-b**). In summary, irrespective of the conformers cyano is a strong electron acceptor, whereas CF_3 and NO_2 act as weak electron acceptors when attached to conformers **a** and **b**, respectively.

3.2.5 Fluorescence energy and lifetime

The fluorescence energies of all BDTs were calculated using TDDFT method, and the results are summarized in Table 4. The fluorescence energies for the highest oscillator strength are assigned to $S_1 \rightarrow S_0$ transition. The examination of the optimized excited state indicates that the excited state of CH_3-substituted BDTs showed negligible structural change with respect to ground state (Table S4 in SI). The excited state of NH_2- and OH-containing BDTs points that the structure is more or less co-planar with respect to the BDT molecule compared to the ground state, due to strong electron-donating effect of NH_2 and OH unit. The change in trend of fluorescence wavelength and oscillator strength is similar to that of the absorption wavelength. The fluorescence peak appears at longer wavelength compared to the absorption peak. This redshift is explained by an increase in the dipole moment in the excited state of the BDTs relative to its ground state (Table 4). The Stokes shift is large for NO_2-substituted BDTs of conformer **b** due to the steric hindrance of the substituent. The Stokes shift is more enlarged for NH_2-2b (0.79) followed by OH-2b (0.63) and CH_3-2b (0.51). In NH_2-2b, steric hindrance of donor and acceptor

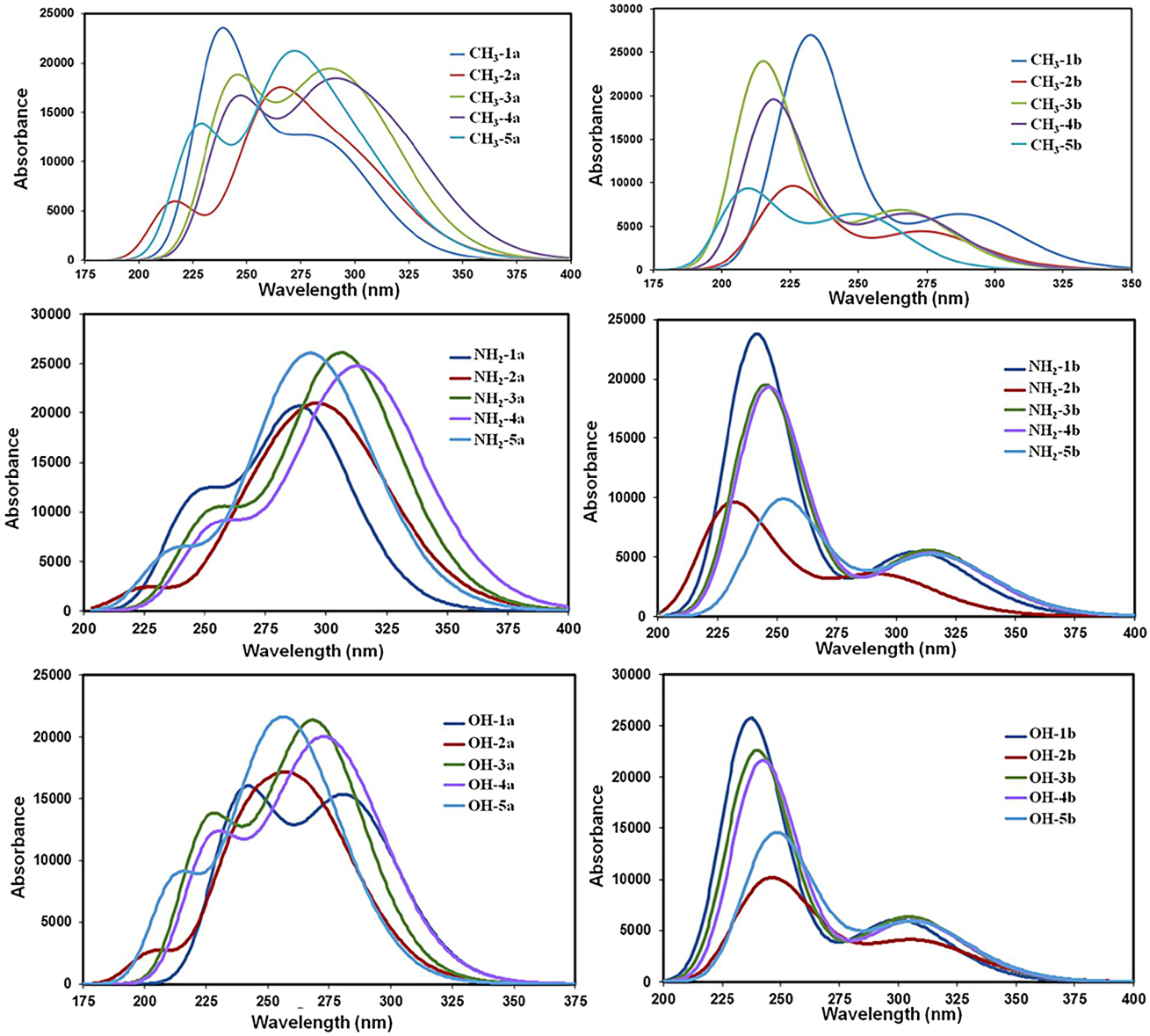

Fig. 6 TDDFT computed absorption spectra of various BDTs using CAM-B3LYP functional and 6-31 + G(d,p) basis set

substituent is strong in the ground state which is compensated during optical excitation enabling the electron delocalization between donor and acceptor ends. The Stokes shift is small in CH_3-2b because the steric hindrance is relatively weak, and only negligible structural changes occur on photoexcitation.

The fluorescence energies and oscillator strengths were used to calculate the radiative lifetimes that are summarized in Table 4. The radiative lifetime (τ in ns) based on the Einstein transition probabilities is expressed as [43],

$$\tau = \frac{c^3}{2E_{flu}^2 f}$$

where c is the velocity of light, E_{flu} is the fluorescence transition energy (in au.), and f is oscillator strength. The predicted radiative lifetimes are shortest for conformer **a** with strong electron acceptors and longest for conformer **b** with weak electron acceptors. The shortest lifetimes are observed for the cyano-substituted BDT and increased in the following fashion as NH_2-3a < OH-3a < CH_3-3a, and their extrapolated lifetimes are 48.86, 56.51, and 75.96 ns, respectively. The lifetime of NH_2-3a is 7.56 and 27.10 ns shorter than that of OH-3a and CH_3-3a, implying that there is longtime emission of electrons in OH-3a and CH_3-3a. In contrast, the florescence lifetimes are significantly increased for nitro-substituted BDT where the values decrease as follows, NH_2 (1435.81) > OH (773.43) > CH_3 (516.36). Particularly,

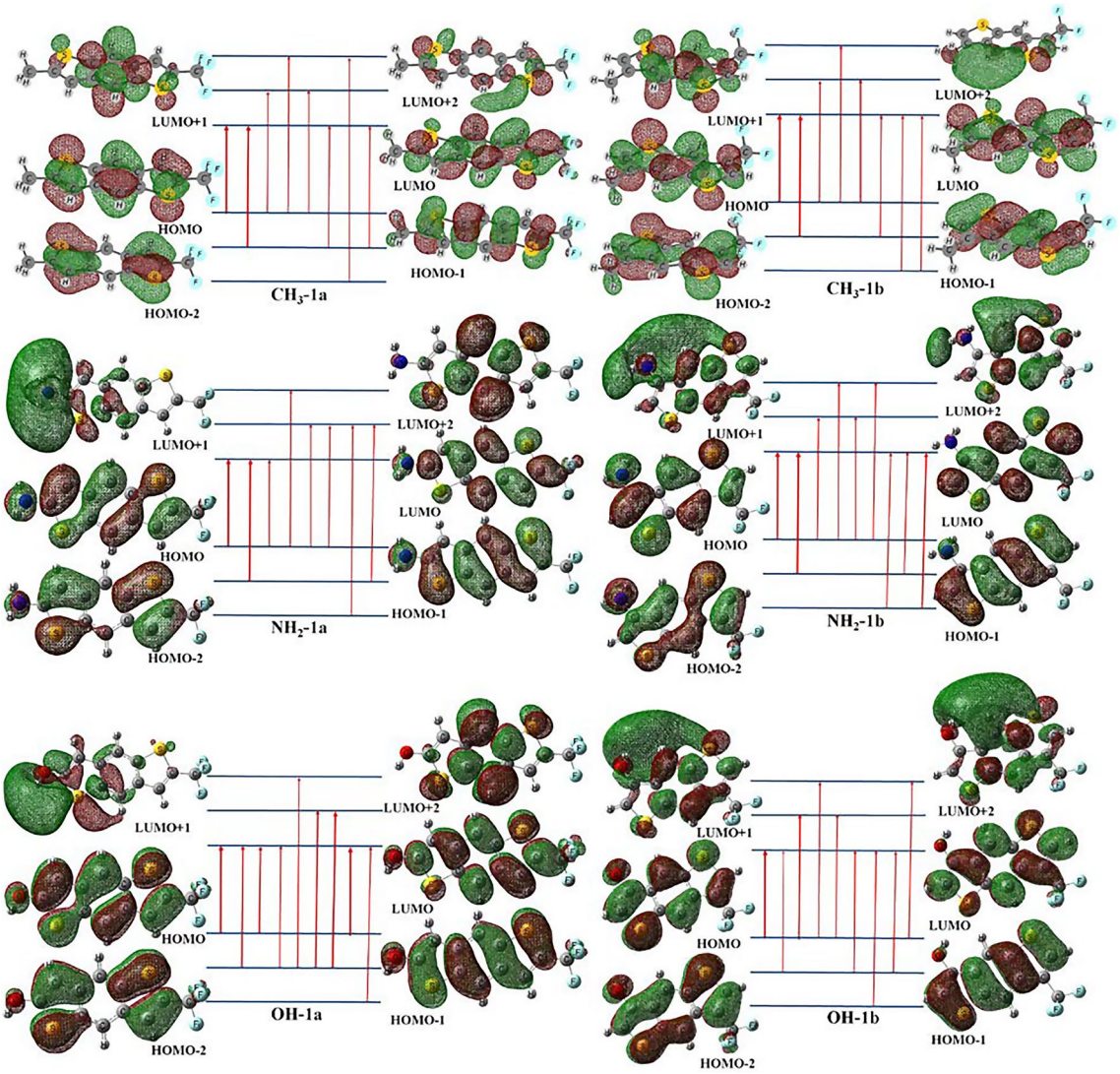

Fig. 7 Computed molecular orbitals involved in transitions for CF_3-substituted BDTs plotted with an isocontour value of 0.2 $Å^{-3}$. Note that for other models the orbital transition diagrams are given in supplementary information, Figs. S7, S8, S9, and S10

NH_2-3a and NH_2-2b exhibit the shortest and longest lifetimes compared to all BDTs studied. These computed data are valuable and would contribute to further design and development of D-A molecules for efficient charge transfer.

3.2.6 Structure–property relationship for optical excitation

The excited state optimization show rotation of the donor and acceptor substituents attached to the BDT molecule. The rotation of the substituent causes it to align with respect to the BDT molecular plane. The improper dihedral angle (ω) is reduced in excited BDT molecules due to substantial rotation during excited state geometry relaxation (Table S4 in SI). The important factor that causes the decrease in ω is the resonance effect between the BDT and the substituent that provides affinity to align with the molecular plane in order to attain enhanced electron delocalization as observed in charge distribution. The decrease in bond length or bond characters from ground and excited states shows the strong bond formation with substituents in excited state (Table S4 in SI). For CH_3-substituted BDTs, the optical-induced structural changes between donor and BDT are small while NH_2-2b and OH-2b show significant structural change. These facts show that the substituents undergo rotation upon photoexcitation enabling charge transfer, as the substituents tend to become more coplanar with the BDT molecule in the excited state.

Table.4 Computed absorption and emission wavelength (λ in nm), molecular orbital contribution, oscillator strength (f), absorption and fluorescence energies (E_{abs} and E_{flu} in eV), ground state and excited state dipole moments (μ_{GS} and μ_{ES} in Debye), fluorescence lifetime (τ in ns), and Stokes shift (in eV) obtained using TDDFT method

	Absorption					Emission						
Conformer	λ	MO contribution	f	E_{abs}	μ_{GS}	λ	MO contribution	f	E_{flu}	μ_{ES}	τ	Stokes shift
CH_3-1a	294.02	H→L (41.11%)	0.2008	4.22	4.55	322.23	H→L (90.99%)	0.3510	3.85	5.14	88.93	0.37
CH_3-1b	290.69	H→L (43.05%)	0.1432	4.27	3.59	316.94	H→L (92.47%)	0.2136	3.91	3.63	141.68	0.36
CH_3-2a	356.93	H→L (45.68%)	0.2224	3.47	7.10	405.31	H→L (92.56%)	0.1999	3.06	7.82	247.17	0.41
CH_3-2b	332.92	H→L (46.42%)	0.1075	3.72	5.77	386.08	H→L (95.13%)	0.0869	3.21	6.03	516.36	0.51
CH_3-3a	308.45	H→L (43.31%)	0.2645	4.02	6.45	340.82	H→L (93.27%)	0.4602	3.64	6.84	75.96	0.38
CH_3-3b	296.07	H→L (43.38%)	0.1564	4.19	5.33	322.14	H→L (87.61%)	0.2083	3.85	5.35	149.92	0.34
CH_3-4a	318.85	H→L (44.92%)	0.2533	3.89	3.31	352.86	H→L (94.23%)	0.3820	3.51	4.04	98.08	0.38
CH_3-4b	298.83	H→L (43.77%)	0.1480	4.15	2.37	328.29	H→L (93.66%)	0.1727	3.78	2.51	187.79	0.37
CH_3-5a	330.22	H→L (44.03%)	0.2257	3.76	5.15	364.94	H→L (90.24%)	0.2324	3.40	5.59	172.21	0.36
CH_3-5b	302.93	H→L (43.88%)	0.1472	4.09	4.35	318.55	H→L (91.88%)	0.1364	3.89	5.17	223.92	0.20
NH_2-1a	292.03	H→L (82.25%)	0.4171	4.25	5.97	327.43	H→L (94.39%)	0.6411	3.79	7.30	50.32	0.46
NH_2-1b	308.84	H→L (90.99%)	0.1331	4.02	4.12	374.15	H→L (93.56%)	0.1178	3.31	4.81	357.61	0.71
NH_2-2a	361.66	H→L (88.18%)	0.4369	3.43	8.79	407.42	H→L (91.96%)	0.5264	3.04	10.39	94.92	0.39
NH_2-2b	349.42	H→L (89.06%)	0.0844	3.55	6.25	449.45	H→L (94.28%)	0.0423	2.76	7.20	1435.81	0.79
NH_2-3a	309.58	H→L (89.63%)	0.5604	4.01	7.96	347.42	H→L (95.19%)	0.7434	3.57	9.19	48.86	0.44
NH_2-3b	314.27	H→L (87.71%)	0.1361	3.95	5.81	379.74	H→L (89.84%)	0.1153	3.27	6.47	376.41	0.68
NH_2-4a	319.54	H→L (88.15%)	0.4779	3.88	4.98	358.92	H→L (94.74%)	0.6615	3.45	6.51	58.63	0.43
NH_2-4b	315.13	H→L (85.44%)	0.1299	3.93	2.86	377.73	H→L (87.81%)	0.1100	3.28	3.66	390.47	0.65
NH_2-5a	329.63	H→L (86.62%)	0.4805	3.76	6.67	367.19	H→L (93.59%)	0.6363	3.38	7.95	63.76	0.38
NH_2-5b	316.95	H→L (81.94%)	0.1249	3.91	4.27	382.98	H→L (86.62%)	0.0936	3.24	5.11	471.73	0.67
OH-1a	287.42	H→L (75.31%)	0.2617	4.31	4.36	319.66	H→L (93.31%)	0.5047	3.88	5.28	60.92	0.43
OH-1b	300.38	H→L (90.29%)	0.1473	4.13	2.78	343.89	H→L (94.33%)	0.1706	3.61	3.09	208.67	0.52
OH-2a	352.58	H→L (89.39%)	0.3225	3.52	6.91	398.27	H→L (92.15%)	0.3730	3.11	7.99	127.99	0.41
OH-2b	338.11	H→L (91.02%)	0.0970	3.67	4.68	407.42	H→L (94.48%)	0.0646	3.04	5.30	773.43	0.63
OH-3a	302.94	H→L (86.60%)	0.3947	4.09	6.18	339.29	H→L (94.93%)	0.6132	3.65	6.96	56.51	0.44
OH-3b	305.10	H→L (88.47%)	0.1538	4.06	4.36	348.22	H→L (92.10%)	0.1688	3.56	4.64	216.14	0.50
OH-4a	313.68	H→L (86.99%)	0.3299	3.95	4.11	350.62	H→L (94.42%)	0.5105	3.54	5.00	72.48	0.41
OH-4b	306.89	H→L (87.16%)	0.1440	4.04	2.96	348.33	H→L (91.44%)	0.1565	3.56	3.24	233.39	0.48
OH-5a	323.76	H→L (85.50%)	0.3286	3.83	5.61	359.41	H→L (92.20%)	0.4521	3.45	6.44	85.98	0.38
OH-5b	308.16	H→L (84.28%)	0.1399	4.02	3.93	328.29	H→L (91.28%)	0.1119	3.78	4.55	289.82	0.24

4 Conclusions

The computational studies on various BDT models show that for CH_3 donor minimal structural change is observed irrespective of the acceptor substitutions, while for NH_2 and OH donors the structural changes are significant. A major variation is also observed in the electronic density distribution. All the molecules show excellent π-conjugation. The computed NPA charges and NICS values indicate the intramolecular charge transfer ~ 0.2 e from the terminal five-membered rings to the acceptor unit. The computed NMR chemical shift values confirm the push–pull behavior of these BDTs. The calculated HOMO–LUMO gap, softness, and hardness parameters indicates highly electronegative CF_3-substituted CH_3-1b is chemically inert and less polarizable while NO_2-substituted NH_2-2a and NH_2-2b become relatively active and more polarizable. Further, the orbital pictures show the strong overlap between ortho-substituted conformers and sulfur lone pair than meta-substituted conformers. The calculated λ_{hole} and λ_{ele} values are small for CH_3-3b-substituted models indicating that cyano group serves as an efficient ambipolar transport system. For NH_2 and OH donors, the NO_2- and CN-substituted BDTs are good candidates for hole and electron transport, respectively. The electron excitation analysis of the BDT models predicts LE for all NO_2-substituted systems, except NH_2-2a which show CT excitation due to deviation of the substituents from the BDT molecular plane. The absorption spectra obtained from TDDFT method point to $\pi \rightarrow \pi^*$ transition in CH_3-substituted BDTs, whereas $\pi \rightarrow \pi^*$ and $n \rightarrow \pi^*$

transitions are dominant in NH_2- and OH-substituted BDTs. Among the models studied here, NO_2-containing BDTs are found to be efficient with longer absorption wavelength. The calculated fluorescence lifetimes were found to be the shortest and longest for cyano- and nitro-substituted BDTs. Finally, the structure–property relationships were explored which revealed a marked reduction of improper dihedral angle (ω) in excited state molecule due to the bond rotation during excited state geometry relaxation. Our study provides useful insights into the structure–property relationship, electronic, and charge transfer properties that would be certainly handy to the experimentalist to carry the quest for better molecules with enhanced properties.

Supplementary Information The online version contains supplementary material available at https://doi.org/10.1007/s00214-021-02855-5.

Acknowledgements G P and D M G thank the Department of Science and Technology-Core Research Grant (DST-CRG), GOI, for funding. K F thanks the Department of Science and Technology (DST), GOI, for the award of Innovation in Science Pursuit for Inspired Research (INSPIRE) Fellowship.

Author contribution Authors KF and DMG have equally contributed the work under the guidance of GP.

References

1. Duan L, Chen J, Liu B, Wang X, Shu W, Yang R (2017) The A-D-A type small molecules with isomeric benzodithiophene cores: synthesis and influence of isomers on photoelectronic properties. Tetrahedron 73:550–557. https://doi.org/10.1016/j.tet.2016.12.044
2. He G, Du L, Gong Y, Liu Y, Yu C, Wei C, Yuan WZ (2019) Crystallization-induced red phosphorescence and grinding-induced blue-shifted emission of a benzobis(1,2,5-thiadiazole)-thiophene conjugate. ACS Omega 4:344–351. https://doi.org/10.1021/acsomega.8b02805
3. Chen X, Liu B, Zou Y, Xiao L, Guo X, He Y, Li Y (2012) A new benzo[1,2-b:4,5-b′]difuran-based copolymer for efficient polymer solar cells. J Mater Chem 22:17724–17731. https://doi.org/10.1039/c2jm32843g
4. Liu B, Chen X, He Y, Li Y, Xu X, Xiao L, Li L, Zou Y (2013) New alkylthienyl substituted benzo[1,2-b:4,5-b′]dithiophene-based polymers for high performance solar cells. J Mater Chem A 1:570–577. https://doi.org/10.1039/c2ta00474g
5. Solomon RV, Veerapandian P, Vedha SA, Venuvanalingam P (2012) Tuning nonlinear optical and optoelectronic properties of vinyl coupled triazene chromophores: a density functional theory and time-dependent density functional theory investigation. J Phys Chem A 116:4667–4677. https://doi.org/10.1021/jp302276w
6. Liu YL, Feng JK, Ren AM (2007) Theoretical study of optical and electronic properties of the bis-dipolar diphenylamino-endcapped oligoarylfluorenes as promising light emitting materials. J Phys Org Chem 20:600–609. https://doi.org/10.1002/poc.1215
7. Kulyk B, Kerasidou AP, Soumahoro L, Moussallem C, Gohier F, Frere P, Sahraoui B (2016) Optimization and diagnostic of nonlinear optical features of π-conjugated benzodifuran-based derivatives. RSC Adv 6:14439–14447. https://doi.org/10.1039/c5ra25889h
8. Ahn M, Kim MJ, Cho DW, Wee KR (2021) Electron push-pull effects on intramolecular charge transfer in perylene-based donor-acceptor compounds. J Org Chem 86:403–413. https://doi.org/10.1021/acs.joc.0c02149
9. Bureš F (2014) Fundamental aspects of property tuning in push-pull molecules. RSC Adv 4:58826–58851. https://doi.org/10.1039/c4ra11264d
10. Getmanenko YA, Fonari M, Risko C, Sandhu B, Galan E, Zhu L, Tongwa P, Hwang DK, Singh S, Wang H, Tiwari SP, Loo YL, Bredas JL, Kippelen B, Timofeeva T, Marder SR (2013) Benzo[1,2-b:6,5-b′]dithiophene(dithiazole)-4,5-dione derivatives: synthesis, electronic properties, crystal packing and charge transport. J Mater Chem C 1:1467–1481. https://doi.org/10.1039/c2tc00805j
11. Xie X, Liu ZH, Bai FQ, Zhang HX (2019) Performance regulation of thieno[3,2-b]benzothiophene π-spacer-based D-π-A organic dyes for dye-sensitized solar cell applications: insights from computational study. Front Chem. https://doi.org/10.3389/fchem.2018.00676
12. Keshtov ML, Marochkin DV, Kochurov VS, Khokhlov AR, Koukaras EN, Sharma GD (2014) New conjugated alternating benzodithiophene-containing copolymers with different acceptor units: synthesis and photovoltaic application. J Mater Chem A 2:155–171. https://doi.org/10.1039/c3ta12967e
13. Figueira-Duarte TM, Müllen K (2011) Pyrene-based materials for organic electronics. Chem Rev 111:7260–7314. https://doi.org/10.1021/cr100428a
14. Li S, Li Y, Song P, Ma F, Yang Y (2017) A DFT study of the structures and photoelectric properties of benzodithiophene-based molecules by replacing sulfur with a variety of heteroatoms (O, N, P, Si, Se). ChemistrySelect 2:3838–3847. https://doi.org/10.1002/slct.201700085
15. Li H, Yi C, Moussi S, Liu S, Daul C, Gratzel M, Decurtins S (2013) Benzo[1,2-b:4,5-b′]difuran-based sensitizers for dye-sensitized solar cells. RSC Adv 3:19798–19801. https://doi.org/10.1039/c3ra43669a
16. Solomon RV, Jagadeesan R, Vedha SA, Venuvanalingam P (2014) A DFT/TDDFT modelling of bithiophene azo chromophores for optoelectronic applications. Dye Pigment 100:261–268. https://doi.org/10.1016/j.dyepig.2013.09.016
17. Liu X, Xu Z, Cole JM (2013) Molecular design of UV-vis absorption and emission properties in organic fluorophores: toward larger bathochromic shifts, enhanced molar extinction coefficients, and greater stokes shifts. J Phys Chem C 117:16584–16595. https://doi.org/10.1021/jp404170w
18. Bourass M, Touimi Benjelloun A, Benzakour M, Mcharfi M, Jhilal F, Serein-Spirau F, Sotiropoulos JM, Bouachrine M (2017) DFT/TD-DFT characterization of conjugational electronic structures and spectral properties of materials based on thieno[3,2-b][1]benzothiophene for organic photovoltaic and solar cell applications. J Saudi Chem Soc 21:563–574. https://doi.org/10.1016/j.jscs.2017.01.001
19. Pavilek B, Kožíšek J, Zalibera M, Luspai K, Gibulkova Z, Koziskova J, Vegh D (2020) Ortho-substituent-controlled regioselective cyclisation of 1,4-phenylenediacrylic acid to a linear benzo[1,2-b:4,5-b′]dithiophene derivative as a building block for semiconducting materials. Tetrahedron Lett. https://doi.org/10.1016/j.tetlet.2020.151608
20. Ghosh D, Periyasamy G, Pati SK (2011) Density functional theoretical investigation of the aromatic nature of BN substituted benzene and four ring polyaromatic hydrocarbons. Phys Chem Chem Phys 13:20627–20636. https://doi.org/10.1039/c1cp22104c

21. Yanai T, Tew DP, Handy NC (2004) A new hybrid exchange-correlation functional using the Coulomb-attenuating method (CAM-B3LYP). Chem Phys Lett 393:51–57. https://doi.org/10.1016/j.cplett.2004.06.011
22. Frisch MJ, Trucks, GW, Schlegel HB, Scuseria GE, Robb MA, Cheeseman JR, Scalmani G, Barone V, Mennucci B, Petersson GA, Nakatsuji H, Caricato M, Li X, Hratchian HP, Izmaylov AF, Bloino J, Zheng G, Sonnenberg JL, Hada M, Ehara M, Toyota K, Fukuda R, Hasega KJ, Cross JB, Bakken V, Adamo C, Jaramillo J, Gomperts R, Stratmann RE, Yazyev O, Austin AJ, Cammi R, Pomelli C, Ochterski JW, Martin RL, Morokuma K ZV, Voth GA, Salvador P, Dannenberg JJ, Dapprich S, Daniels AD, Farkas O, Foresman JB, Ortiz JV, Cioslowski J FD (2009) Gaussian 09, Revision D. Gaussian, Inc Wallingford, CT
23. Reed AE, Weinhold F (2017) Intermolecular interactions from a natural bond orbital, donor-acceptor viewpoint. Chem Rev 88:899–926
24. Reed AE, Weinstock RB, Weinhold F (1985) Natural population analysis. J Chem Phys 83:735–746. https://doi.org/10.1063/1.449486
25. Pearson RG (1986) Absolute electronegativity and hardness correlated with molecular orbital theory. Proc Natl Acad Sci 83:8440–8441. https://doi.org/10.1073/pnas.83.22.8440
26. Schleyer PVR, Maerker C, Dransfeld A, Jiao H, Eikema Hommes NJR (1996) Nucleus-independent chemical shifts: a simple and efficient aromaticity probe. J Am Chem Soc 118:6317–6318. https://doi.org/10.1021/ja960582d
27. Wolinski K, Hinton JF, Pulay P (1990) Efficient implementation of the gauge-independent atomic orbital method for NMR chemical shift calculations. J Am Chem Soc 112:8251–8260. https://doi.org/10.1021/ja00179a005
28. Lu T, Chen F (2012) Multiwfn: a multifunctional wavefunction analyzer. J Comput Chem 33:580–592. https://doi.org/10.1002/jcc.22885
29. Liu Z, Lu T, Chen Q (2020) An sp-hybridized all-carboatomic ring, cyclo[18]carbon: electronic structure, electronic spectrum, and optical nonlinearity. Carbon N Y 165:461–467. https://doi.org/10.1016/j.carbon.2020.05.023
30. Lu T (2021) Multiwfn-A multifunctional wavefunction analyzer, Software Manual, version 3.8 (dev). http://sobereva.com/multiwfn
31. Dreuw A, Head-Gordon M (2005) Single-reference ab initio methods for the calculation of excited states of large molecules. Chem Rev 105:4009–4037. https://doi.org/10.1021/cr0505627
32. Li T-C, Tong P (1986) Time-dependent density-functional theory for multicomponent systems. Phys Rev A 34:529–532. https://doi.org/10.1103/PhysRevA.34.529
33. Michael K (1950) Characterization of electronic transitions in complex molecules. Discuss Faraday Soc 9:14–19
34. Valencia D, Whiting GT, Bulo RE, Weckhuysen BM (2016) Protonated thiophene-based oligomers as formed within zeolites: understanding their electron delocalization and aromaticity. Phys Chem Chem Phys 18:2080–2086. https://doi.org/10.1039/c5cp06477e
35. Marcus RA (1993) Electron transfer reactions in chemistry: theory and experiment (Nobel Lecture). Angew Chem Int Ed Engl 32:1111–1121. https://doi.org/10.1002/anie.199311113
36. Rana B, Periyasamy G, Bhattacharya A (2016) On the ultrafast charge migration dynamics in isolated ionized halogen, chalcogen, pnicogen, and tetrel bonded clusters. Chem Phys. https://doi.org/10.1016/j.chemphys.2016.02.018
37. Calvo-Castro J, McHugh CJ, McLean AJ (2015) Torsional angle dependence and switching of inner sphere reorganisation energies for electron and hole transfer processes involving phenyl substituted diketopyrrolopyrroles; A density functional study. Dye Pigment 113:609–617. https://doi.org/10.1016/j.dyepig.2014.09.031
38. Le Bahers T, Adamo C, Ciofini I (2011) A qualitative index of spatial extent in charge-transfer excitations. J Chem Theory Comput 7:2498–2506. https://doi.org/10.1021/ct200308m
39. Guido CA, Cortona P, Mennucci B, Adamo C (2015) Relation between nonlinear optical properties of push-pull molecules and metric of charge transfer excitations. J Chem Theory Comput 11:4182–4188. https://doi.org/10.1021/acs.jctc.5b00538
40. Adamo C, Le Bahers T, Savaresea M, Wilbrahama L, García G, Fukudaf R, Eharaf M, Rega N, Ciofini I (2015) Exploring excited states using time dependent density functional theory and density-based indexes. Coord Chem Rev 304–305:166–178. https://doi.org/10.1016/j.ccr.2015.03.027
41. Rubio A, Marques M (2009) Time-dependent density-functional theory. Phys Chem Chem Phys 11:4436. https://doi.org/10.1039/b908105b
42. Wiggins P, Williams JAG, Tozer DJ (2009) Excited state surfaces in density functional theory: a new twist on an old problem. J Chem Phys. https://doi.org/10.1063/1.3222641
43. Bransden BH, Joachain CJ (1983) Physics of atoms and molecules. Longman, London, UK